catalysts

MDPI

Article

Effect of Hydrogen-Donor of Heavy Crude Oil Catalytic Aquathermolysis in the Presence of a Nickel-Based Catalyst

Khoshim Kh. Urazov [1,*], Nikita N. Sviridenko [1,*], Yuliya A. Iovik [1], Ekaterina N. Kolobova [2], Maria V. Grabchenko [3], Irina A. Kurzina [4] and Irek I. Mukhamatdinov [5]

1 Institute of Petroleum Chemistry, Siberian Branch of the Russian Academy of Sciences, 4 Akademicheskiy Ave., 634055 Tomsk, Russia
2 Research School of Chemistry and Applied Biomedical Sciences, Tomsk Polytechnic University, 30 Lenin Ave., 634050 Tomsk, Russia
3 Laboratory of Catalytic Research, Tomsk State University, 36 Lenin Ave., 634050 Tomsk, Russia
4 Faculty of Chemistry, Tomsk State University, 36 Lenin Ave., 634050 Tomsk, Russia
5 Institute of Geology and Petroleum Technologies, Kazan Federal University, 18 Kremlyovskaya Str., 420008 Kazan, Russia
* Correspondence: urazovhh@gmail.com (Kh.Kh.U.); nikita26sviridenko@gmail.com (N.N.S.)

Abstract: The transformations of oil components from the Zyuzeevskoye field during catalytic aquathermolysis in the presence of a nickel-containing catalyst precursor and hydrogen donors were studied. It was found that the yield of gasoline and diesel fractions increased by more than 36% in the case of catalytic aquathermolysis in the presence of tetralin. The maximum conversion of asphaltenes was achieved with a simultaneous slowing down of coke formation by four times. The calculation of the structural-group parameters of initial asphaltenes and the products of thermal cracking and catalytic aquathermolysis was made, and the hypothetical construction of their molecular structures was proposed. It was established that the phase composition, ratio, and morphology of nickel catalysts after catalytic aquathermolysis (CA) and catalytic aquathermolysis with tetralin (CA+T) depend on the amount of "free" hydrogen and are represented by $Ni_{0.96}S$ and Ni_9S_8.

Keywords: heavy oil; fractional composition; asphaltenes; elemental analysis; XRD; SEM; structural group analysis

Citation: Urazov, K.K.; Sviridenko, N.N.; Iovik, Y.A.; Kolobova, E.N.; Grabchenko, M.V.; Kurzina, I.A.; Mukhamatdinov, I.I. Effect of Hydrogen-Donor of Heavy Crude Oil Catalytic Aquathermolysis in the Presence of a Nickel-Based Catalyst. *Catalysts* **2022**, *12*, 1154. https://doi.org/10.3390/catal12101154

Academic Editor: Jose Maria Arandes

Received: 9 September 2022
Accepted: 27 September 2022
Published: 1 October 2022

1. Introduction

Despite the active development of renewable energy sources, the resource of crude oil remains still a major contributor to the energy sector. According to forecasts, the average daily oil consumption by 2040 will increase to 109.4 million barrels. The depletion of the reserves of light and medium oils is forcing oil refineries to switch to hydrocarbon raw materials such as heavy and extra heavy oil [1–5]. However, their processing according to the classical schemes of thermal and catalytic cracking has proven to be unprofitable due to the high content of resin–asphaltene substances (RASs) [6–8]. The presence of these components in the structure, primarily asphaltenes, S, N, and O heteroatoms, among others, causes their tendency to condense on the active sites of catalysts [7,8]. This prevents their transformation into liquid products, and, accordingly, leads to a decrease in the yield of valuable fractions. In addition, polycondensation products accumulate on the pieces of the equipment, which ultimately leads to a decrease in its service life. Hence, there is an urgent need to develop catalytic systems for heavy oil feedstock processing, the main task of which will be to reduce the content of asphaltenes and increase the yield of light fractions [9].

The large production of marketable oil products from heavy hydrocarbon feedstock is impossible since it is characterized by a low H/C ratio. Since the use of widely accepted hydrotreatment with the purpose to increase this ratio is economically unviable, the catalytic aquathermolysis of heavy oil seems to be a promising method. In this process, water acts

as a hydrogen donor and also a hydrocarbon solvent [10]. Active hydrogen is formed due to the water–gas shift (WGS) reaction [10], and water dissociation on the catalyst surface [11]. However, the efficiency of converting water into hydrogen is low [2]. Despite the fact that, after catalytic aquathermolysis, the viscosity of heavy oils decreases, secondary condensation processes can occur with the formation of resins and asphaltenes and an increase in viscosity. Various hydrogen donors can close the active chains formed during the catalytic aquathermolysis of heavy oil [12–16].

In general, the use of hydrogen donors makes it possible not only to increase the yield of light fractions but also to suppress the processes of coke formation [17,18]. Not only water but also formic acid [19], methane [20], isopropanol [21,22], cyclohexane [23], tetralin [24], decalin [25], and other substances [26] can be used as donors. The efficiency of their use depends on a number of factors, such as the nature of the oil [27], the catalyst, and the conditions for upgrading [24,28]. In a number of works, hydrogen donors (tetralin and decalin) and gaseous hydrogen were compared during the cracking of heavy oil in the presence of nickel–molybdenum catalysts [24,29]. The results suggest the efficiency of using hydrogen donors to upgrade oil with a low coke yield. This is due to the fact that atomic hydrogen, unlike molecular hydrogen, arrests the polymerization of free radicals with the formation of stable and low molecular weight molecules.

To achieve the maximum effect from upgrading heavy oil in the presence of a hydrogen donor, it is worth taking into account the H-donor index and the hydrogen transfer index. The effect of the use of naphthalene derivatives on the composition of products of the vacuum residue cracking was described by [30]. It was shown that the efficiency of these compounds as hydrogen donors increased in the following order: 1-methylnaphthalene < decalin < naphthalene < tetralin. The obtained data correlated with the values of the H-donor index, where it was the highest for tetralin. Jia-Kai Bai et al. found a relationship between the activity of hydrogen donors and the structure of their molecules [31]. An analysis of the diagram of the highest occupied molecular orbitals (HOMOs) of tetralin showed the presence of hyperconjugation between the C_α-H bond and the π bond of the benzene ring, which resulted in the delocalization of the σ electrons in the C_α-H bond to the benzene ring and the weakening of the C_α-H bond. The fact that tetralin has the highest hydrogen transfer rate among all naphthalene derivatives was also confirmed by the results obtained by Sung-Ho Kim et al. [30]. The reactions of hydrogen formation from tetralin and decalin can be expressed as follows:

Generally, the dehydrogenation of decalin (Scheme 1) includes a few simultaneous, reversible reaction pathways: tetralin formation from decalin and the conversion of tetralin to naphthalene.

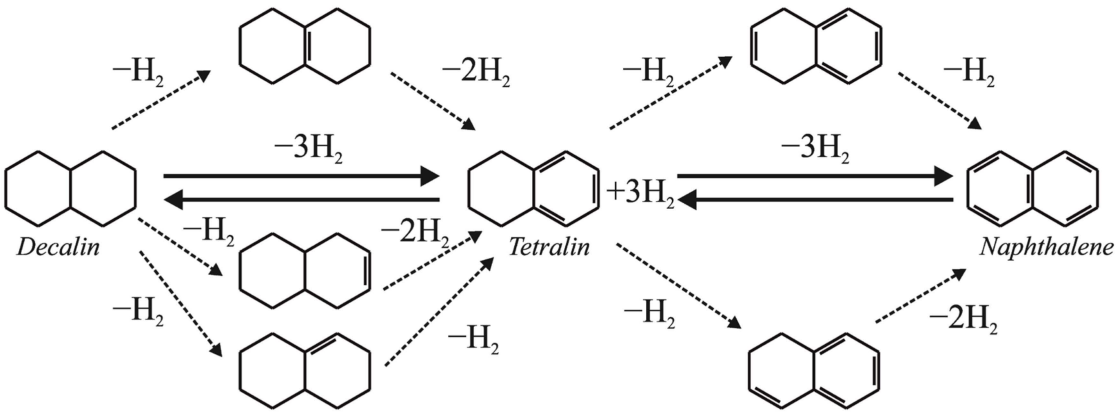

Scheme 1. Possible reaction mechanism of decalin dehydrogenation. Adapted with permission from Ref. [28] (2022, Elsevier).

Ameen A. Al-Muntaser et al. [32] demonstrated the effect of aquathermolysis conditions on the composition of heavy oil-cracking products. It was found that an increase in

the heat treatment temperature led to a decrease in the viscosity and density of oil due to the deep destruction of the resin–asphaltene components. In this case, sample losses due to gas and coke formation were found to be high. The use of dispersed catalysts and water-soluble catalyst precursors can significantly improve the quality of heavy oil aquathermolysis products; however, their removal and subsequent reuse are fundamentally difficult [33]. The prospects of using the compounds of transition group metals (Ni, Co, Fe, Mo, and others) for these purposes are described in [6,33–38]. Nickel compounds are of particular interest because of their high activity in the degradation of resin–asphaltene components and the absence of problems with diffusion, which in turn leads to efficient contact between the reagents and the catalyst [39–41]. Alfiya Lakhova et al. [9] demonstrated the efficiency of using nickel nanoparticles in the cracking of Athabasca oil. The researchers suggested that the use of a nanosized nickel catalyst in the cracking of super heavy oil accelerated the destruction of asphaltenes, which resulted in a significant decrease in its viscosity [34]. However, it was shown that the use of these catalysts also resulted in an increase in the yield of not only light fractions but also by-products, in particular, coke [18]. Aquathermolysis in the presence of a nickel catalyst (nanocompounds with the Keggin structure) made it possible to suppress polymerization reactions, thereby reducing the viscosity of heavy oil by 96% [42].

The aim of this work was to determine the yield of light fractions, the transformation of oil components, and the nature of structural-group changes in asphaltene molecules in the case of the in situ catalytic aquathermolysis of heavy oil in the presence of hydrogen donors.

2. Results and Discussion

It was revealed that the introduction of additives of tetralin (T) and decalin (D) in both the thermal cracking (C) and catalytic aquathermolysis (CA) of heavy oil resulted in an increase in the yield of gaseous products (Table 1). In the CA, CA+T, and C+T experiments, the yield of condensation products was reduced by a factor of 2–4, compared with conventional cracking. It should be noted that the use of tetralin in aquathermolysis (CA+T) made it possible not only to slow down the coke formation but also to increase the destruction of asphaltenes with the formation of mainly resins. The obtained results once again confirmed the effectiveness of using this additive as an H-donor, which prevented the interaction of radicals with each other and, accordingly, the formation of molecules with a large molecular weight [43]. By contrast, the addition of decalin to the cracked system accelerated the condensation reactions, so the coke content increased by 1.5–2 wt.% in the cases of both aquathermolysis and cracking (C+D and CA+D). Additionally, in both cases, significant sample losses were observed, since the total yield of by-products is about 13%.

Table 1. Yield of products in the catalytic aquathermolysis of heavy oil in the presence of hydrogen donors.

Indices	Initial Oil	Experiment					
		C	CA	CA+T	C+T	CA+D	C+D
Gas yield, wt.%		5.0	5.8	5.6	6.9	7.9	8.2
- Sulfur content in gas, wt.%		0.64	1.41	1.91	1.18	1.15	1.20
Coke yield, wt.%		3.4	1.8	0.8	1.2	5.2	4.9
- Sulfur content in coke, wt.%		0.14	0.11	0.03	0.09	0.39	0.28
Liquid products (LP), wt.%	100	91.6	92.4	93.6	91.9	86.9	86.9
- Sulfur content in LP, wt.%	4.53	3.75	3.01	2.59	3.26	2.99	3.05
SARA, wt.%							
Saturates+aromatics	68.1	74.7	75.2	74.9	70.5	70.4	71.7
Resins	21.5	11.0	10.2	13.1	14.4	12.5	11.5
Asphaltenes	10.4	5.9	7.0	5.6	7.0	4.0	3.7

The maximum depth of the desulfurization of liquid products was observed in the CA+T experiment. This result was probably due to the fact that the active hydrogen formed according to Scheme 2 promoted the hydrodesulfurization reaction, where sulfur-containing gases were among its products. Indirectly, this assumption confirmed the increase in their yield by a factor of three, compared with experiment C, and two times, compared with CA. Thus, the simultaneous presence of a nickel catalyst and water and tetralin acting as hydrogen donors in the system had the most effective effect on sulfur removal.

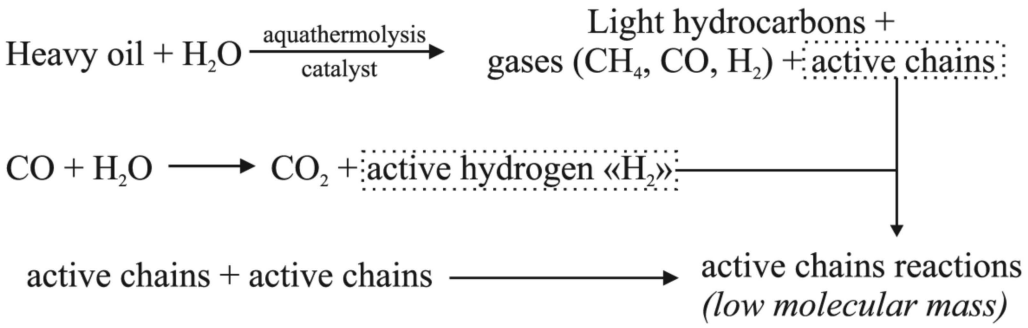

Scheme 2. Pathways of active hydrogen formation during aquatemolysis.

According to the data presented in Figure 1, the fractional composition of oil after thermal cracking changed as follows: the content of fractions boiling away in the temperature range of ibp–200 °C increased from 13.5 to 22.0 wt.%, while the content of 200–360 °C distillate increased from 17.3 to 28.6 wt.%. Both additives considered in this work (C+T and C+D) affected the yield of light fractions insignificantly. After CA, the yield of light fractions increased to 59.3 wt.%. The residual fraction (IBP > 500 °C) decreased by 12.9% compared with thermal cracking and by 27.2% compared with the initial oil. This suggested that the high molecular weight components of the feedstock underwent deep degradation in the case of catalytic aquathermolysis. The use of tetralin in this process (CA+T) made it possible to increase the yield of fractions boiling up to 360 °C to 67.2 wt.%. This was probably due to the active hydrogenation of radicals formed upon breaking the C–C, C–S, and C–O bonds of resin and asphaltene molecules. Smaller amounts of distillate components evaporating in the ranges IBP–200 and 200–360 °C were observed in the CA+D experiment. Hence, the content of distillate increased only by 1.3 and 4.7 wt.%, respectively, which was presumably due to the low values of the H-donor index of decalin [43].

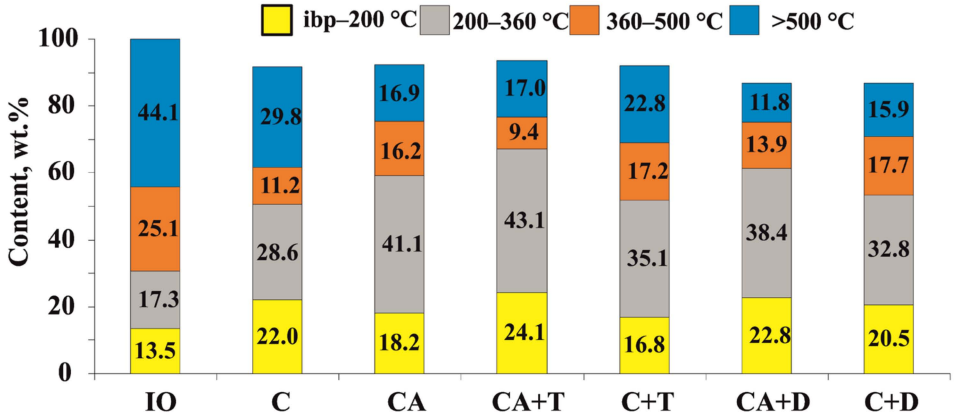

Figure 1. Fractional composition of the products of catalytic aquathermolysis of heavy oil in the presence of hydrogen donors.

The results of determining the elemental composition of asphaltenes indicated that the conditions of cracking (the presence or absence of water in the system), as well as the

use of additives, insignificantly affected the distribution of C, H, and N atoms in their structure [44]. Probably, during thermal and catalytic cracking, alkyl substituents were removed, and the aromatization of naphthenic cycles of molecules occurred, which caused a decrease in their H/C ratio (Table 2).

Table 2. Elemental composition of initial asphaltene and after catalytic aquathermolysis of heavy oil.

Asphaltenes	Content, wt.%					
	C	H	N	S	O	H/C
Initial oil	80.01	7.63	1.81	5.51	5.04	1.144
C	79.56	5.78	2.31	5.46	6.89	0.872
CA	79.78	5.75	2.21	7.25	5.01	0.865
CA+T	81.49	6.10	2.25	7.16	3.00	0.898
C+T	81.06	5.79	1.95	7.54	3.66	0.857
CA+D	80.15	5.54	2.04	7.67	4.60	0.829
C+D	80.15	5.64	1.92	7.51	4.78	0.844

Table 3 presents the calculated structural-group parameters of the initial asphaltenes and the products of C, CA, CA+T, and C+T cracking, on the basis of which the spatial structures of their molecules were constructed (Figure 2).

Table 3. Average physicochemical and structural parameters of the initial asphaltenes molecules and the products of non-catalytic and catalytic aquathermolysis.

Parameters	Initial Oil	C	CA	CA+T	C+T
MM, a.m.u.	1920	782	851	863	828
Number of atoms in a mean molecule					
C	128.0	51.8	56.6	58.6	55.9
H	146.5	45.2	48.9	52.6	47.9
N	2.5	1.3	1.3	1.4	1.2
S	3.3	1.3	1.9	1.9	2.0
O	6.0	3.4	2.7	1.6	1.9
Number of rings					
R_T	24.8	13.1	14.9	14.6	14.3
R_{Ar}	15.5	9.6	11.3	10.3	10.8
R_N	9.3	3.5	3.6	4.3	3.5
m_a	3.81	1.89	1.10	1.47	1.35
σ_a	0.56	0.41	0.45	0.46	0.40
Number of carbon atoms of different types in a mean molecule					
C_{Ar}	62.0	34.3	36.5	37.3	37.3
C_N	32.4	12.4	12.6	16.2	10.6
C_S	33.6	5.2	7.5	5.1	8.0
n	3.56	2.49	2.79	2.50	2.63
f_a	48.5	66.1	64.5	63.6	66.7

MM is the molecular mass; C_{Ar} is the number of carbon atoms in aromatic rings; C_N is the number of carbon atoms in naphthenic rings; C_S is the number of carbon atoms in aliphatic fragments of the mean molecule. R_T is the total number of rings, R_{Ar} is the number of aromatic rings, and R_N is the number of saturated rings. f_a is the aromaticity factor, σ_a is the degree of substitution of aromatic cores, m_a is the number of blocks in a molecule, and n is average length of alkyl substituents.

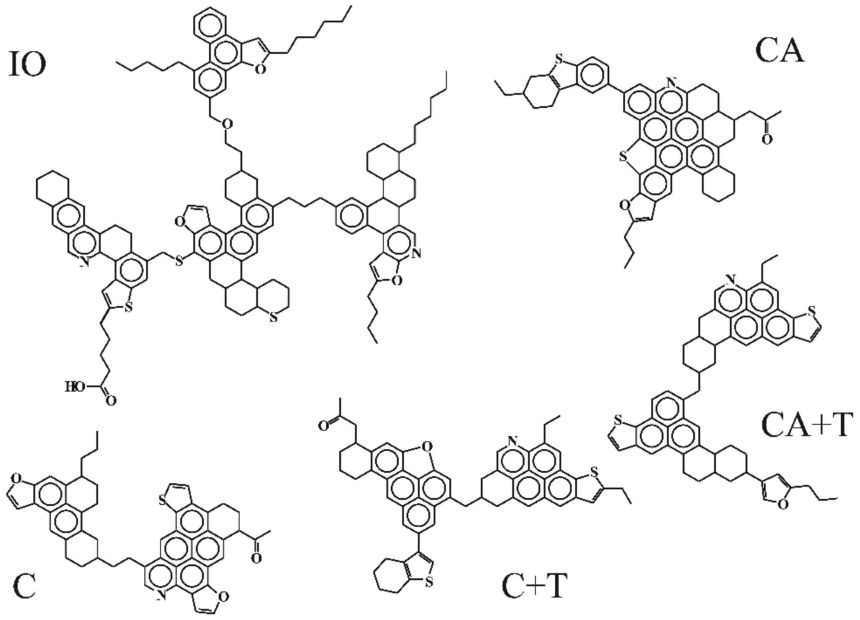

Figure 2. Hypothetical structures of asphaltenes of initial oil and products of cracking.

The asphaltenes isolated from the initial oil were a mixture of hetero-organic molecules mainly consisting of four blocks with an average composition of $C_{128}H_{146.5}N_{2.5}S_{3.3}O_6$ and a molecular mass of 1920 a.m.u. (Table 3). The structural block of such a mean molecule consists of 33–34 carbon atoms combined into 6 naphthenic-aromatic cycles. It was revealed that the percentage of carbon atoms enclosed in aromatic structures was almost half of their total number, being equal to 48.5%. In particular, there were two or three naphthenic cycles for each aromatic core. The total number of carbon atoms in the alkyl fragments of one average block (C_S*) was 8.8, and the alkyl chain length (n) did not exceed 3.56. The initial asphaltenes also contained from two to three nitrogen atoms, three sulfur atoms, and up to six oxygen atoms. It followed from this that each of their structural blocks conventionally accounted for 0.65 N* atoms, 0.87 S* atoms, and 1.57 O* atoms. Presumably, such a distribution of heteroatoms indicated that the asphaltenes under consideration contained a significant amount of the functional groups of carboxylic acids and ester bridges connecting the structural blocks of molecules.

The asphaltenes obtained after the thermal cracking of oil significantly differed in their characteristics. Their mean molecules were heteroorganic two-block structures with an average composition of $C_{51.8}H_{45.2}N_{1.3}S_{1.3}O_{3.4}$ and an average molecular mass of 782 a.m.u. In this case, there were about 27 carbon atoms per structural block, i.e., 6–7 less than for the asphaltenes of the initial oil. Due to aromatization reactions, the average number of cycles in one block increased from 6.5 to 6.9 (the amount of R^*_{Ar} increased, while R^*_N decreased), respectively, while the aromaticity factor increased to 66.1%. The number of carbon atoms in aliphatic fragments and their average length decreased from 33.6 to 5.2 and from 3.56 to 2.49, respectively, which suggested the active dealkylation and cyclization reactions. According to the data in Table 3, the total content of N and O in the mean molecule of the asphaltenes of C products decreased by two times, while the content of S by three times. Thus, each structural block contained N* and S* by 0.69 and O* by 1.80. The larger values of N* and O* indicated that the formation of asphaltenes proceeded, among other things, due to the condensation of high-molecular nitrogen- and oxygen-containing compounds.

After catalytic aquathermolysis, the asphaltenes became single-block structures with an average composition of $C_{56.6}H_{48.9}N_{1.3}S_{1.9}O_{2.7}$ and MM of 851 a.m.u. Their structural blocks were enlarged due to condensation and aromatization reactions. Hence, the total number of rings was 14.9, 11.3 rings of which were aromatic. The number of carbon atoms in them also naturally increased (by four in comparison with C asphaltenes). In the

course of CA, the reactions of dealkylation proceeded less intensively than during thermal cracking, which is indicated by the larger values of C_S and n (7.5 and 2.79, respectively). The number of heteroatoms per average structural block of the asphaltene molecule also significantly increased.

The use of tetralin in the CA process resulted in the production of asphaltenes with similar MM values (851 and 863 a.m.u.). However, these asphaltenes were significantly different in their structure. They were composed of heteroorganic monoblock and diblock molecules with an average composition of $C_{58.6}H_{52.6}N_{1.4}S_{1.9}O_{1.6}$. Their average structural block consisted of 10 cycles, with R^*_{Ar} equal to 7 and R^*_N equal to 3. An increase in the content of naphthenic rings together with a decrease in aromatic rings suggested, on the one hand, the occurrence of hydrogenation reactions, and, on the other hand, a slowdown in aromatization reactions. The similar values of C_S and n for the asphaltenes obtained after CA+T and C suggested that the dealkylation of alkyl fragments in these processes proceeded at approximately the same rate. It should be noted that the addition of tetralin did not affect the distribution of N and S atoms (compared with CA asphaltenes), while the oxygen content decreased by one atom (from 2.7 to 1.6).

The analysis of the diffraction patterns (Figure 3) of solid products after CA and CAT showed the presence of $Ni_{0.96}S$ and Ni_9S_8 nickel sulfide phases. During CA, the nickel-containing catalyst was sulfided by the sulfur components of the oil to form $Ni_{0.96}S$ (PDF 00-050-1791). The reflections of weak intensity at 2Θ = 31.2, 50.6, and 73.1° suggested the presence of the Ni_9S_8 phase (PDF 00-022-1193). The average CSR value, estimated from the most pronounced reflection, was 15.89 nm and 16.72 nm for $Ni_{0.96}S$ and Ni_9S_8, respectively. Catalytic aquathermolysis in the presence of tetralin was accompanied by the formation of well-crystallized $Ni_{0.96}S$ (PDF 00-050-1791) and Ni_9S_8 (PDF 00-022-1193) phases, the CSR values of which were found to be 24.00 nm and 11.98 nm, respectively.

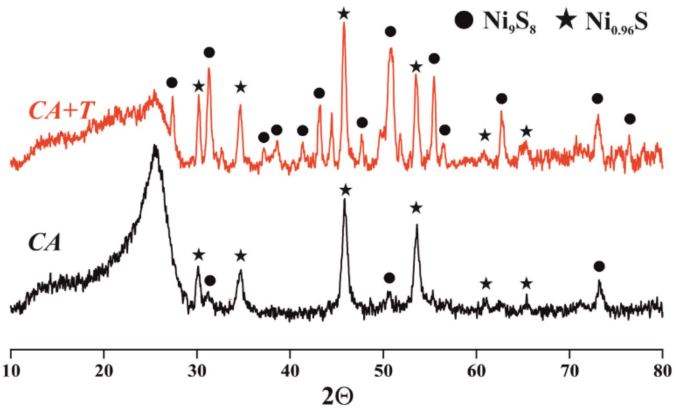

Figure 3. X-ray diffraction patterns of coke-containing catalysts.

Probably, at the first stage of the cracking process, nickel oxide interacted with oil sulfur compounds. The resulting Ni_9S_8 disproportionated into $Ni_{0.96}S$ and $Ni_{x-0.96}S_6$. Then, the $Ni_{x-0.96}S_6$ phase was sulfided by sulfur-containing components to Ni_9S_8 [45]. With the accumulation of the $Ni_{0.96}S$ phase, which was the end product of the sulfidation of the Ni-containing catalyst (Scheme 3), the desulfurization of oil slowed down. Consequently, the depth of oil desulfurization was affected by the ratio of the $Ni_{0.96}S$ and Ni_9S_8 phases, as well as the amount of hydrogen sulfide and "free" hydrogen in the reaction medium [46].

Figures 4 and 5 show the SEM images of a coke-containing catalyst. In the course of CA and CA+T, the condensation of asphaltene molecules resulted in the formation of sponge-like coke [47,48]. This was presumably due to the occurrence of decarboxylation and dehydrogenation reactions accompanied by the evolution of gaseous products. A decrease in the intensity of reflection at 2Θ = 25.4° of the CA+T condensation products suggested that the presence of tetralin in the reaction medium promoted the formation of coke, which was more hydrogen-enriched than coke in the case of CA (Figure 3). In

addition, when using T, spherical nickel particles were formed, which, according to the literature data, is due to the processes of hydrogen redistribution in the system [49].

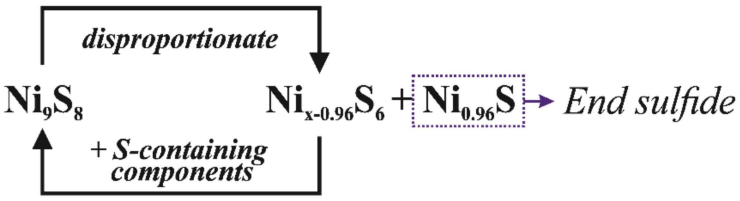

Scheme 3. Formation of catalytically active nickel sulfide.

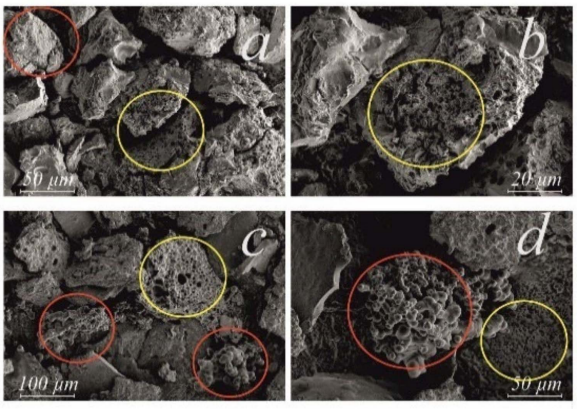

Figure 4. SEM images of the coke-containing catalyst: CA ((**a**) 50 μm and (**b**) 20 μm) and CA+T ((**c**) 10 μm and (**d**) 50 μm). Red circles—Ni_xS_y; yellow circles—sponge-like coke.

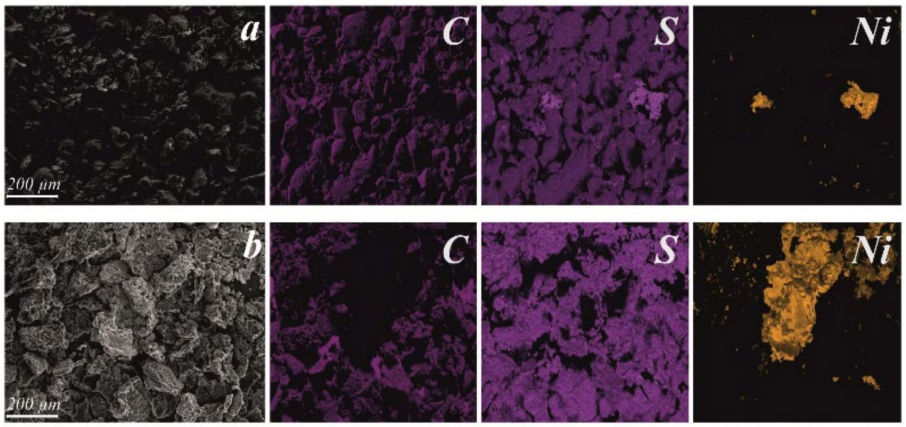

Figure 5. SEM images and elemental mapping from the surface of coke-containing catalysts: (**a**) C+T and (**b**) CA+T.

The mapping of the surface of the coke-containing catalyst isolated after CA showed an inhomogeneous distribution of the sulfur and nickel, the formation of which required the ratio S:Ni ≈ 1 (Figure 5a). After CA+T, the distribution of sulfur on the surface was more uniform, which could contribute to the formation of the two phases of nickel sulfides (Figure 5b). This was probably due to the presence of a larger amount of hydrogen in the reaction medium.

XPS analysis was carried out to study the chemical state of Ni and S after CA and CA+T coke-containing catalysts (Figure 6). As shown in Figure 6, for both samples, the Ni 2p spectra showed two spin-orbit doublets accompanied by two shake-up satellites ("Sat"). The analysis of the spectra showed that two photoelectron peaks for Ni $2p_{3/2}$ and Ni $2p_{1/2}$ at 856 eV and 872.7 eV corresponded to the state of Ni^{2+} [50]. These values of binding

energy (BE) indicated that Ni_xS_y on the surface was in an oxidized state due to its contact with moisture and oxygen in the air. In the S2p spectra, in addition to the peaks associated with sulfur–metal bonds (163.3 eV and 164.25 eV), spectra related to sulfur–oxygen bonds (168.5 eV) [51] were also observed as a result of their interaction with air [52].

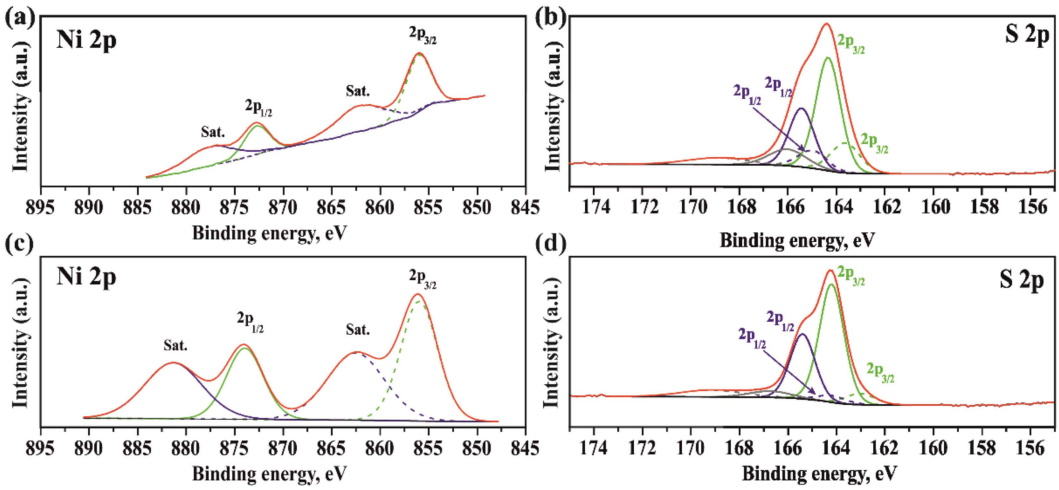

Figure 6. XPS spectra of coke-containing catalyst after CA (**a**,**b**) and CA+T (**c**,**d**).

3. Research Methods

For this research, we selected the oil of Zyuzeevskoye field (Tatarstan Republic), with the following physicochemical properties (Table 4): this oil is heavy (class I—ρ = 934–966 kg/m^3), with a low content of light fractions, with especially high sulfur (> to 3.5 wt.% according to GOST 51858-2002).

Table 4. Physical and chemical properties of the initial heavy oil.

Characteristics	Zyuzeevskoye Field
Density at 20 °C, kg/m^3	940.0
Dynamic viscosity, mPa s—at 20 °C	743
Elemental composition, wt.%	
- Carbon	81.01
- Hydrogen	11.45
- Sulfur	4.53
- Nitrogen	0.89
- Oxygen	2.12
- H/C	1.69
Component composition, wt.%	
- Saturated hydrocarbons	24.6
- Aromatic hydrocarbons	43.5
- Resins	21.5
- Asphaltenes	10.4
Fractional composition, wt.%	
- ibp-200 °C	13.5
- 200–360 °C	17.3
- 360–500 °C	25.1
- >500 °C	44.1

The laboratory modeling of the aquathermolysis process was carried out in an autoclave with a volume of 12 cm^3 (Figure 7). The weight of the heavy oil loaded into the reactor was 7 g, and those of the water additives were up to 2 wt.%. The nickel catalyst precursor

and the hydrogen donor were introduced at 0.4 wt.% and 5.0 wt.%, respectively [37]. The experiments were carried out at a temperature of 450 °C and duration of 80 min.

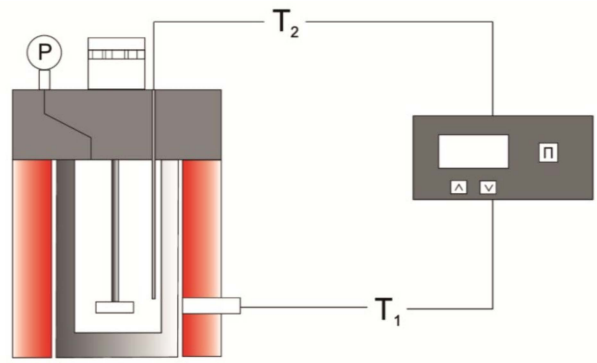

Figure 7. Schematic diagram of an oil-cracking unit.

The physicochemical properties of the feedstock and the products of cracking were determined in accordance with the ASTM standards. The kinematic viscosity was determined using a rotational viscometer. The content of saturated, aromatic hydrocarbons, resins, and asphaltenes (SARA components) was determined by the method described in ASTM D4124. The sulfur content was measured according to ASTM-D4294, and distillation curves were obtained according to ASTM-D2887.

The elemental analysis of the samples was performed using a "Vario EL Cube" CHNS analyzer at a temperature of 1150 °C. The CHNS analyzer's operating principle is based on the classical technique of burning the sample in a quartz tube in an oxygen medium, where O analysis is a method of recovery in the atmosphere He/H_2. The analysis was carried out on the emitted gases on a katharometer using the method of displacement chromatography, and the separation of gases on a chromatographic column. The absolute error of the analyzer did not exceed ±0.1 % for each element being determined. The oxygen content was evaluated from the difference between 100 % and the sum of the C, H, N, and S elements. The molecular mass (MM) was measured via cryoscopy in naphthalene. The ^1H NMR spectra were recorded using a Bruker AVANCE AV 300 NMR–Fourier spectrometer at 300 MHz. The asphaltenes samples were dissolved in deuterated chloroform ($CDCl_3$). The obtained ^1H-NMR spectra were divided into four zones (H_{Ar}, H_α, H_β, and H_γ) in accordance with the chemical shifts in hydrogen atoms presented in Table 5 [53].

Table 5. Assignments of hydrogen atoms in ^1H NMR spectra.

Type of Hydrogen	Chemical Shift (ppm)	Assignments
H_{Ar}	6.5–9.5	aromatic hydrogen
H_α	2.0–4.5	α hydrogen of aliphatic chains
H_β	1.0–2.0	β hydrogen of aliphatic chains
H_γ	0.5–1.0	γ hydrogen of aliphatic chains

The average structural parameters were calculated according to the Brown–Ladner empirical formulas based on the ^1H-NMR and elemental analysis data and the MM values (Table 6) described in the work of Sun et al. [54].

The phase composition of the catalytic additive was investigated via X-ray phase analysis (a Bruker D8 XRD powder diffractometer, a Lynx Eye detector, and monochrome CuKα radiation). The morphology of the samples was investigated using a Thermo Fisher Scientific Apreo S LoVac scanning electron microscope with the EDS+EDBS analysis system at an accelerating voltage of 30 kV. The elemental composition of the sample surface was analyzed using the Octane Elect EDS system and APEX software.

Table 6. Calculated formulas for the asphaltene structural parameters (ASPs).

Symbol	Structure Parameters	Calculated Formulas
H_T	Total hydrogen numbers	$M_w \times H\%$
C_T	Total carbon numbers	$(M_w \times C\%)/12$
n	Average alkyl chain length	$(H_\alpha + H_\beta + H_\gamma)/H_\alpha$
f_a	Aromaticity factor	$(C/H - H_\alpha/2 - H_\beta/2 - H_\gamma/2)/(C/H)$
H_{AU}/C_{Ar}	Condensation degree parameter of the aromatic ring	$(H_\alpha/2 + H_{Ar})/(C/H - H_\alpha/2 - H_\beta/2 - H_\gamma/2)$
σ	Replacement rate of periphery hydrogen in the aromatic ring system	$(H_\alpha/2)/(H_\alpha/2 + H_{Ar})$
C_{Ar}	Aromatic carbon numbers	$f_a \times C_T$
C_s	Saturated carbon numbers	$C_T - C_{Ar}$
C_{ap}	Peripheral carbon in a fused aromatic ring	$C_{Ar} \times H_{AU}/C_{Ar}$
C_i	Internal carbon in a fused aromatic ring	$C_{Ar} - C_{ap}$
$C_{Ar(us)}$	Aromatic carbon number per unit structure	$(2.503/H_{AU}/C_{Ar})^2$
u	Blocks number in molecule	C_{Ar} / $C_{Ar(us)}$
R_T	Total rings	$C_T - H_T/2 + 1 - C_{Ar}/2$
R_{Ar}	Aromatic rings	$C_{Ar}/2 - (H_\alpha \times H_T)/4 - (H_{Ar} \times H_T)/2 + 1$
R_N	Naphthenic rings	$R_T - R_{Ar}$

X-ray photoelectron spectroscopy (XPS) was applied for a study of the oxidation state of nickel and sulfur using a Thermo Fisher Scientific XPS NEXSA spectrometer with a monochromated Al K-α X-ray source (1486.6 eV) and equipped with a flood gun for the charge compensation. The survey spectra were recorded with a pass energy rate of 200 eV and a step size of 1 eV, while a pass energy rate of 50 eV and a step size of 0.1 eV were applied for the high-resolution spectra. The analyzed area was 200 μm^2. The charging shifts were referenced against adventitious carbon at the binding energy (BE) of 285 eV. It should be noted that XPS provides information about the electronic/chemical state of elements only in the near-surface layer (5–15 nm), the composition of which can change during the reaction and upon contact with the environment. The CASA XPS software (version 2.3.15, CASA Software Ltd., Teignmouth, UK, http://www.casaxps.com/, (accessed on 1 September 2022)) was used for processing the spectra.

4. Conclusions

It was found that during the catalytic aquathermolysis of heavy oil, tetralin promoted the slowdown of coke formation and the deep destruction of asphaltenes and sulfur compounds. In this case, the yield of fractions boiling up to 360 °C was about 70 wt.%.

The molecular mass of asphaltenes in the initial oil after CA and CA+T decreased from 1920 to ≈850 a.m.u. The distribution of heteroatoms in their composition changed significantly. The average structure of the initial asphaltenes included three sulfur and nitrogen atoms and up to six oxygen atoms. If after CA, the content of individual heteroatoms decreased by 2–3 times, then the use of tetralin in this process decreased the number of oxygen atoms by 4 times. As a result of CA+T, the share of carbon atoms in the paraffinic and naphthenic fragments of asphaltenes decreased. Conversely, it increased in aromatic fragments. The nickel-containing catalysts in the course of CA and CA+T were sulfided by the sulfur-containing compounds of heavy oil with the formation of $Ni_{0.96}S$ and Ni_9S_8. Thus, it was shown that tetralin affects the ratio and morphology of the formed phases of nickel sulfides.

Author Contributions: Conceptualization, N.N.S.; methodology, I.I.M.; investigation, E.N.K., M.V.G., and I.A.K.; data curation, Kh.Kh.U.; writing—original draft preparation, Yu.A.I. and N.N.S.; writing—review and editing, Kh.Kh.U. All authors have read and agreed to the published version of the manuscript.

Funding: This work was supported by the Ministry of Science and Higher Education of the Russian Federation (Project No. FWRN-2021-0005).

Data Availability Statement: Not applicable.

Acknowledgments: SEM analysis of samples was carried out using the equipment (Thermo Fisher Scientific Apreo S LoVac) of the "NANOTECH" Collective Use Center of the Institute of Strength Physics and Materials Science of the Siberian Branch of the Russian Academy of Sciences. XPS measurements were carried out at the Central laboratories of Tomsk Polytechnic University (Analytical Center).

Conflicts of Interest: The authors declare no conflict of interest.

References

1. REN21. *Renewables 2020 Global Status Report* (INIS-FR–20-1110). France. 2020. Available online: https://www.globalwomennet.org/wp-content/uploads/2020/06/GSR2020_Full_Report_with_Endnotes.pdf (accessed on 1 September 2022).
2. Zhou, Z.; Slaný, M.; Kuzielová, E.; Zhang, W.; Ma, L.; Dong, S.; Zhang, J.; Chen, G. Influence of Reservoir Minerals and Ethanol on Catalytic Aquathermolysis of Heavy Oil. *Fuel* **2022**, *307*, 121871. [CrossRef]
3. Morelos-Santos, O.; Reyes de la Torre, A.I.; Melo-Banda, J.A.; Schacht-Hernández, P.; Portales-Martínez, B.; Soto-Escalante, I.; José-Yacamán, M. A Novel Direct Method in One-Step for Catalytic Heavy Crude Oil Upgrading Using Iron Oxide Nanoparticles. *Catal. Today* **2022**, *392–393*, 60–71. [CrossRef]
4. Li, Z.; Li, Y.; Xu, H.; Jarvis, J.; Meng, S.; Song, H. Effect of Methane Presence on Catalytic Heavy Oil Partial Upgrading. *Fuel* **2021**, *297*, 120733. [CrossRef]
5. Hosseinpour, M.; Hajialirezaei, A.H.; Soltani, M.; Nathwani, J. Thermodynamic Analysis of In-Situ Hydrogen from Hot Compressed Water for Heavy Oil Upgrading. *Int. J. Hydrog. Energy* **2019**, *44*, 27671–27684. [CrossRef]
6. Rana, M.S.; Sámano, V.; Ancheyta, J.; Diaz, J.A.I. A Review of Recent Advances on Process Technologies for Upgrading of Heavy Oils and Residua. *Fuel* **2007**, *86*, 1216–1231. [CrossRef]
7. Kang, K.H.; Kim, G.T.; Park, S.; Seo, P.W.; Seo, H.; Lee, C.W. A Review on the Mo-Precursors for Catalytic Hydroconversion of Heavy Oil. *J. Ind. Eng. Chem.* **2019**, *76*, 1–16. [CrossRef]
8. León, A.Y.; Guzmán, M.A.; Picón, H.; Laverde, C.D.; Molina, V.D. Reactivity of Vacuum Residues by Thermogravimetric Analysis and Nuclear Magnetic Resonance Spectroscopy. *Energy Fuels* **2020**, *34*, 9231–9242. [CrossRef]
9. Lakhova, A.; Petrov, S.; Ibragimova, D.; Kayukova, G.; Safiulina, A.; Shinkarev, A.; Okekwe, R. Aquathermolysis of Heavy Oil Using Nano Oxides of Metals. *J. Pet. Sci. Eng.* **2017**, *153*, 385–390. [CrossRef]
10. Djimasbe, R.; Varfolomeev, M.A.; Al-Muntaser, A.A.; Yuan, C.; Feoktistov, D.A.; Suwaid, M.A.; Kirgizov, A.J.; Davletshin, R.R.; Zinnatullin, A.L.; Fatou, S.D.; et al. Oil Dispersed Nickel-Based Catalyst for Catalytic Upgrading of Heavy Oil Using Supercritical Water. *Fuel* **2022**, *313*, 122702. [CrossRef]
11. Grabchenko, M.; Pantaleo, G.; Puleo, F.; Kharlamova, T.S.; Zaikovskii, V.I.; Vodyankina, O.; Liotta, L.F. Design of Ni-Based Catalysts Supported over Binary La-Ce Oxides: Influence of La/Ce Ratio on the Catalytic Performances in DRM. *Catal. Today* **2021**, *382*, 71–81. [CrossRef]
12. Zhao, F.; Liu, Y.; Wu, Y.; Zhao, X.; Tan, L. Study of Catalytic Aquathermolysis of Heavy Oil in the Presence of a Hydrogen Donor. *Chem. Technol. Fuels Oils* **2012**, *48*, 273–282. [CrossRef]
13. Chen, G.; Yuan, W.; Yan, J.; Meng, M.; Guo, Z.; Gu, X.; Zhang, J.; Qu, C.; Song, H.; Jeje, A. Zn(II) Complex Catalyzed Coupling Aquathermolysis of Water-Heavy Oil-Methanol at Low Temperature. *Pet. Chem.* **2018**, *58*, 197–202. [CrossRef]
14. Chen, G.; Yuan, W.; Bai, Y.; Zhao, W.; Gu, X.; Zhang, J.; Jeje, A. Ethanol Enhanced Aquathermolysis of Heavy Oil Catalyzed by a Simple Co(II) Complex at Low Temperature. *Pet. Chem.* **2017**, *57*, 389–394. [CrossRef]
15. Philippov, A.A.; Chibiryaev, A.M.; Martyanov, O.N. Catalyzed Transfer Hydrogenation by 2-Propanol for Highly Selective PAHs Reduction. *Catal. Today* **2021**, *379*, 15–22. [CrossRef]
16. Chesnokov, V.V.; Dik, P.P.; Nikityonok, A.V.; Chichkan, A.S.; Parmon, V.N. Comparative Analysis of the Effects of Hydrogen and Formic Acid on the Vacuum Residue Hydrocracking. *Chem. Eng. J.* **2022**, *449*, 137839. [CrossRef]
17. Hart, A.; Leeke, G.; Greaves, M.; Wood, J. Down-hole heavy crude oil upgrading by CAPRI: Effect of hydrogen and methane gases upon upgrading and coke formation. *Fuel* **2014**, *119*, 226–235. [CrossRef]
18. Kayukova, G.P.; Mikhailova, A.M.; Feoktistov, D.A.; Morozov, V.P.; Vakhin, A.V. Conversion of the Organic Matter of Domanic Shale and Permian Bituminous Rocks in Hydrothermal Catalytic Processes. *Energy Fuels* **2017**, *31*, 7789–7799. [CrossRef]
19. Hosseinpour, M.; Fatemi, S.; Ahmadi, S.J.; Oshima, Y.; Morimoto, M.; Akizuki, M. Isotope Tracing Study on Hydrogen Donating Capability of Supercritical Water Assisted by Formic Acid to Upgrade Heavy Oil: Computer Simulation vs. Experiment. *Fuel* **2018**, *225*, 161–173. [CrossRef]
20. Safaei Mahmoudabadi, Z.; Rashidi, A.; Panahi, M. New Approach to Unsupported ReS_2 Nanorod Catalyst for Upgrading of Heavy Crude Oil Using Methane as Hydrogen Source. *Int. J. Hydrogen Energy* **2021**, *46*, 5270–5285. [CrossRef]
21. Zhao, F.; Xu, T.; Zhu, G.; Wang, K.; Xu, X.; Liu, L. A Review on the Role of Hydrogen Donors in Upgrading Heavy Oil and Bitumen. *Sustain. Energy Fuels* **2022**, *6*, 1866–1890. [CrossRef]
22. Stepacheva, A.; Gavrilenko, A.; Markova, M.; Semenova, A.; Monzharenko, M.; Sulman, M. The Use of Supercritical Solvents in Crude Oil Fraction Conversion. *J. Phys. Conf. Ser.* **2020**, *1658*, 12057. [CrossRef]

23. Hart, A.; Lewis, C.; White, T.; Greaves, M.; Wood, J. Effect of Cyclohexane as Hydrogen-Donor in Ultradispersed Catalytic Upgrading of Heavy Oil. *Fuel Process. Technol.* **2015**, *138*, 724–733. [CrossRef]
24. Ovalles, C.; Vallejos, C.; Vasquez, T.; Rojas, I.; Ehrman, U.; Benitez, J.L.; Martinez, R. Downhole Upgrading of Extra-Heavy Crude Oil Using Hydrogen Donors and Methane under Steam Injection Conditions. *Pet. Sci. Technol.* **2003**, *21*, 255–274. [CrossRef]
25. Alemán-Vázquez, L.O.; Cano-Domínguez, J.L.; García-Gutiérrez, J.L. Effect of Tetralin, Decalin and Naphthalene as Hydrogen Donors in the Upgrading of Heavy Oils. *Procedia Eng.* **2012**, *42*, 532–539. [CrossRef]
26. Fang, D.; Wang, G.; Sheng, Q.; Ge, S.; Gao, C.; Gao, J. Preparation of Hydrogen Donor Solvent for Asphaltenes Efficient Liquid-Phase Conversion via Heavy Cycle Oil Selective Hydrogenation. *Fuel* **2019**, *257*, 115886. [CrossRef]
27. Ovalles, C.; Rivero, V.; Salazar, A. Downhole Upgrading of Orinoco Basin Extra-Heavy Crude Oil Using Hydrogen Donors under Steam Injection Conditions. Effect of the Presence of Iron Nanocatalysts. *Catalysts* **2015**, *5*, 286–297. [CrossRef]
28. Al-Muntaser, A.A.; Varfolomeev, M.A.; Suwaid, M.A.; Saleh, M.M.; Djimasbe, R.; Yuan, C.; Zairov, R.R.; Ancheyta, J. Effect of Decalin as Hydrogen-Donor for in-Situ Upgrading of Heavy Crude Oil in Presence of Nickel-Based Catalyst. *Fuel* **2022**, *313*, 122652. [CrossRef]
29. Hart, A.; Adam, M.; Robinson, J.P.; Rigby, S.P.; Wood, J. Tetralin and Decalin H-Donor Effect on Catalytic Upgrading of Heavy Oil Inductively Heated with Steel Balls. *Catalysts* **2020**, *10*, 393. [CrossRef]
30. Kim, S.H.; Kim, K.D.; Lee, H.; Lee, Y.K. Beneficial Roles of H-Donors as Diluent and H-Shuttle for Asphaltenes in Catalytic Upgrading of Vacuum Residue. *Chem. Eng. J.* **2017**, *314*, 1–10. [CrossRef]
31. Bai, J.K.; Zhang, X.B.; Li, W.; Wang, X.B.; Du, Z.Y.; Li, W.Y. Rate Constant of Hydrogen Transfer from H-Donor Solvents to Coal Radicals. *Fuel* **2022**, *318*, 123621. [CrossRef]
32. Al-Muntaser, A.A.; Varfolomeev, M.A.; Suwaid, M.A.; Yuan, C.; Chemodanov, A.E.; Feoktistov, D.A.; Rakhmatullin, I.Z.; Abbas, M.; Domínguez-Álvarez, E.; Akhmadiyarov, A.A.; et al. Hydrothermal Upgrading of Heavy Oil in the Presence of Water at Sub-Critical, near-Critical and Supercritical Conditions. *J. Pet. Sci. Eng.* **2020**, *184*, 106592. [CrossRef]
33. Muraza, O.; Galadima, A. Aquathermolysis of Heavy Oil: A Review and Perspective on Catalyst Development. *Fuel* **2015**, *157*, 219–231. [CrossRef]
34. Liu, H.; Wang, J.; Wang, Z.; Fan, S.; Chen, K. Hydrogenation of Nickel Octaethylporphyrin over Dispersed MoS_2 Catalysts Formed In Situ. *ChemistrySelect* **2018**, *3*, 4292–4297. [CrossRef]
35. Alkhaldi, S.; Husein, M.M. Hydrocracking of Heavy Oil by Means of in Situ Prepared Ultradispersed Nickel Nanocatalyst. *Energy Fuels* **2014**, *28*, 643–649. [CrossRef]
36. Chianelli, R. Catalysis Reviews: Science and Engineering Fundamental Studies of Transition Metal Sulfide Hydrodesulfurization Catalysts. *Catal. Rev.* **1984**, *26*, 361–393. [CrossRef]
37. Urazov, K.K.; Sviridenko, N.N. NiO Based Catalysts Obtained "in-Situ" for Heavy Crude Oil Upgrading: Effect of NiO Precursor on the Catalytic Cracking Products Composition. *J. Taiwan Inst. Chem. Eng.* **2021**, *127*, 151–156. [CrossRef]
38. Avbenake, O.P.; Al-Hajri, R.S.; Jibril, B.Y. Saturates and Aromatics Characterization in Heavy Crude Oil Upgrading Using Ni–Co/γ-Al_2O_3 Catalysts. *Pet. Sci. Technol.* **2020**, *38*, 800–807. [CrossRef]
39. Sviridenko, N.N.; Golovko, A.K.; Kirik, N.P.; Anshits, A.G. Upgrading of Heavy Crude Oil by Thermal and Catalytic Cracking in the Presence of NiCr/WC Catalyst. *J. Taiwan Inst. Chem. Eng.* **2020**, *112*, 97–105. [CrossRef]
40. Morelos-Santos, O.; Reyes de la Torre, A.I.; Melo-Banda, J.A.; Mendoza-Martínez, A.M.; Schacht-Hernández, P.; Portales-Martínez, B.; Soto-Escalante, I.; Domínguez-Esquivel, J.M.; José-Yacamán, M. Dispersed Nickel-Based Catalyst for Enhanced Oil Recovery (EOR) Under Limited Hydrogen Conditions. *Top. Catal.* **2020**, *63*, 504–510. [CrossRef]
41. Okunev, A.G.; Parkhomchuk, E.V.; Lysikov, A.I.; Parunin, P.D.; Semeikina, V.S.; Parmon, V.N. Catalytic Hydroprocessing of Heavy Oil Feedstocks. *Russ. Chem. Rev.* **2015**, *84*, 981–999. [CrossRef]
42. Wu, C.; Lei, G.L.; Yao, C.J.; Gai, P.Y.; Cao, Y.B.; Li, X.N. Mechanism for Reducing the Viscosity of Extra-Heavy Oil by Aquathermolysis with an Amphiphilic Catalyst. *Ranliao Huaxue Xuebao/J. Fuel Chem. Technol.* **2010**, *38*, 684–690. [CrossRef]
43. Hart, A.; Leeke, G.; Greaves, M.; Wood, J. Downhole heavy crude oil upgrading using CAPRI: Effect of steam upon upgrading and coke formation. *Energy Fuels* **2014**, *28*, 1811–1819. [CrossRef]
44. Urazov, K.K.; Sviridenko, N.N. Structural Transformations of Heavy Oil Asphaltenes from the Zyuzeevskoye Field upon Thermocatalytic Cracking. *Solid Fuel Chem.* **2022**, *56*, 128–132. [CrossRef]
45. Waldner, P. Fe-Solubility of Ni7S6 and Ni9S 8: Thermodynamic Analysis. *J. Chem. Thermodyn.* **2011**, *43*, 315–318. [CrossRef]
46. Li, Q.; Wang, X.; Zhang, R.; Mi, J.; Wu, M. Insights into the Effects of Metal-Ion Doping on the Structure and Hot-Coal-Gas Desulfurization Properties of Zn-Based Sorbents Supported on SBA-15. *Fuel* **2022**, *315*, 123198. [CrossRef]
47. Picón-Hernández, H.J.; Centeno-Hurtado, A.; Pantoja-Agreda, E.F. Morphological Classification of Coke Formed from the Castilla and Jazmín Crude Oils. *CTyF-Cienc. Tecnol. Future* **2008**, *3*, 169–183. [CrossRef]
48. Crelling, J.C. Coal Carbonization. *Appl. Coal Petrol.* **2008**, 173–192. [CrossRef]
49. Nguyen, M.T.; Nguyen, D.L.T.; Xia, C.; Nguyen, T.B.; Shokouhimehr, M.; Sana, S.S.; Grace, A.N.; Aghbashlo, M.; Tabatabaei, M.; Sonne, C.; et al. Recent Advances in Asphaltene Transformation in Heavy Oil Hydroprocessing: Progress, Challenges, and Future Perspectives. *Fuel Process. Technol.* **2021**, *213*, 106681. [CrossRef]
50. Gao, Q.; Luo, W.; Ma, X.; Ma, Z.; Li, S.; Gou, F.; Shen, W.; Jiang, Y.; He, R.; Li, M. Electronic Modulation and Vacancy Engineering of Ni_9S_8 to Synergistically Boost Efficient Water Splitting: Active Vacancy-Metal Pairs. *Appl. Catal. B Environ.* **2022**, *310*, 121356. [CrossRef]

51. Chen, L.; Deng, W.; Chen, Z.; Wang, X. Hetero-Architectured Core-Shell $NiMoO_4$@Ni_9S_8/MoS_2 Nanorods Enabling High-Performance Supercapacitors. *J. Mater. Res.* **2022**, *37*, 284–293. [CrossRef]
52. Hussain, S.; Ullah, N.; Zhang, Y.; Shaheen, A.; Javed, M.S.; Lin, L.; Zulfiqar; Shah, S.B.; Liu, G.; Qiao, G. One-Step Synthesis of Unique Catalyst Ni_9S_8@C for Excellent MOR Performances. *Int. J. Hydrog. Energy* **2019**, *44*, 24525–24533. [CrossRef]
53. Fergoug, T.; Bouhadda, Y. Determination of Hassi Messaoud Asphaltene Aromatic Structure from 1H & 13C NMR Analysis. *Fuel* **2014**, *115*, 521–526. [CrossRef]
54. Sun, Y.D.; Yang, C.H.; Zhao, H.; Shan, H.H.; Shen, B.X. Influence of Asphaltene on the Residue Hydrotreating Reaction. *Energy Fuels* **2010**, *24*, 5008–5011. [CrossRef]